

<https://doi.org/10.1038/s44172-026-00639-y>

Determining the percentage of recycled plastic content in a plastic product



Yaoli Zhao¹, Charuvahan Adhivarahan², Chandra Lekha Jyothula¹, Karthik Dantu², Thomas Thundat¹ & Amit Goyal¹ ✉

As global plastic waste continues to rise, accurately identifying and quantifying recycled content in plastic products is critical for developing a circular economy. At present, there is no method that can accurately determine the percentage of recycled plastic content in a plastic product. Here, we demonstrate a multi-modal, non-destructive sensing technique to determine the percentage of recycled plastic in plastic products. We have developed a multi-modal, multi-physics approach that integrates triboelectric properties, dielectric/impedance spectroscopy, capacitance measurements, mid-infrared spectroscopy, combined with machine learning and artificial intelligence to quantify the recycled content in plastics. Experimental results reveal that increasing recycled content leads to enhanced charge retention, reduced permittivity, and increased dielectric loss, consistent with polymer chain scission and defect-induced polarization. The machine learning model trained on the multi-modal dataset achieves we achieved over 97% classification accuracy across PET samples ranging from 0% to 50% recycled content, which is the expected regime of required recycled content in plastic products. This method offers a solution for control and regulatory compliance for recycled plastics.

Each year, approximately 400 million tons of plastic waste are generated worldwide, yet only ~9% of this waste is effectively recycled¹. The first part of the 5th session of the Intergovernmental Negotiating Committee (INC-5.1) to finalize an international legally binding agreement to end plastic pollution, including in the marine environment, was held in Busan, Republic of Korea, in December 2024², involving participants from 170 nations and 440 organizations. While a legally binding agreement was not reached, the delegates agreed to meet again as the second part of the 5th session (INC 5.2) to arrive at a legally binding agreement to end plastics pollution in 2025 at Geneva, Switzerland³. It is widely expected that recycling and reuse of plastics in a circular manner will be a major contributor to realize this goal of ending plastics pollution. It is expected that there will be policy regulations mandating a certain percentage of recycled plastic content in most plastic products. However, besides conducting an audit of starting materials used to fabricate a plastic product, no technique exists that allows the determination of the percentage of recycled plastic content in a plastic product.

There are many analytical techniques to characterize various physical aspects of plastics, such as Fourier Transform Infrared Spectroscopy (FTIR)⁴, Thermogravimetric Analysis (TGA)⁵, Differential Scanning Calorimetry (DSC)⁶, and Nuclear Magnetic Resonance (NMR)⁷.

Additionally, mechanical and electrical tests evaluate flammability, impact resistance, tensile strength, and dielectric performance^{8–11}, providing characterization of material properties. However, none of these techniques can quantify the proportion of recycled content in a finished product. In addition, tracer-based approaches have been proposed, in which fluorescent or elemental markers are added to recycled materials to facilitate downstream quantification^{12,13}. However, the number of PET products currently incorporating such tracers is extremely low, limiting the feasibility of using tracer-based methods for widespread quantification across the plastics value chain. This limitation poses significant challenges for manufacturers, policymakers, and consumers seeking to verify compliance with regulations that require a minimum percentage of recycled content¹⁴. The lack of a device that can determine the percentage of recycled content in a plastic product restricts the ability to monitor and enforce sustainability policies effectively.

In addition, as plastics are reused or recycled, their chemical and physical properties degrade. Understanding and quantifying the proportion of recycled plastic in commercial products is critical to ensuring material quality and compliance with emerging regulatory policies aimed at promoting a circular economy. Recycled plastics exhibit inferior mechanical,

¹Department of Chemical and Biological Engineering (CBE), School of Engineering and Applied Sciences (SEAS), University at Buffalo, Buffalo, NY, USA.

²Department of Computer Science and Engineering (CSE), School of Engineering and Applied Sciences (SEAS), University at Buffalo, Buffalo, NY, USA.

✉ e-mail: agoyal@buffalo.edu

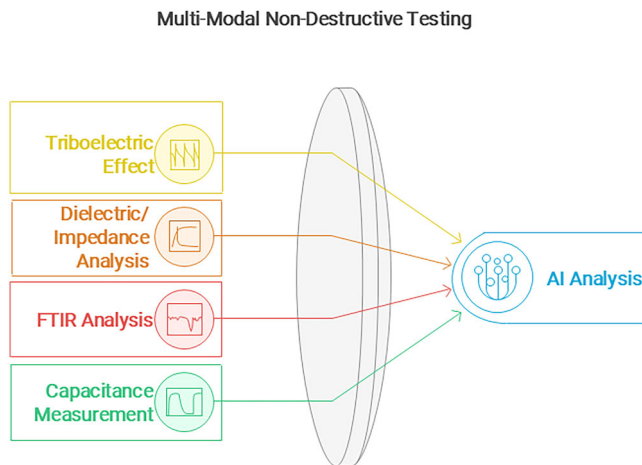


Fig. 1 | Schematic diagrams show multi-modal and multi-physics technique for characterizing recycled content in plastics. Although results from individual, disparate techniques cannot be used for the accurate determination of the percentage of recycled content in plastic products, analyzing the dataset generated by the various techniques using AI and ML shows accurate prediction of recycled content.

viscoelastic, dielectric, thermal, and chemical properties compared to virgin resins due to polymer chain scission, oxidation, and contamination introduced during multiple recycling cycles^{15,16}. Plastics consist of long molecular chains that provide a high strength-to-weight ratio, but repeated processing, including extrusion, molding, and reprocessing, results in chain fragmentation and property degradation¹⁷. Unlike metals, which can be indefinitely recycled with minimal loss in properties, polymers experience cumulative structural changes, which limit their recyclability and affect their usability in high-performance applications¹⁸.

Determining the percentage of recycled plastic in a plastic product is technically challenging since the chemical nature of the polymer does not change during recycling. However, recycled plastics exhibit distinct electrical and spectroscopic signatures due to electrically active defects resulting from polymer chain fragmentation^{19–21}. Here, we propose a multi-modal and multi-physics sensing technique that enables rapid testing of recycled plastic content in a plastic product, as illustrated in Fig. 1. Our approach integrates triboelectric charging and discharging analysis, dielectric/impedance analysis, capacitance analysis, and mid-infrared spectroscopy to extract electrical, dissipative, and chemical properties of plastic materials. By leveraging these complementary sensing techniques, our method captures a comprehensive dataset that reflects the structural and compositional differences between virgin and recycled plastics. Combined with machine learning (ML) and artificial intelligence (AI) our technique allows an accurate quantification of the recycled percentage of plastic in a plastic product.

Triboelectric analysis reveals that higher recycled content correlates with increased charge retention, likely due to polarization of electrically active defects²². Dielectric and impedance spectroscopy show that recycled plastics display a decrease in permittivity and an increase in dielectric loss, suggesting reduced polarization and enhanced energy dissipation^{23,24}. Capacitance analysis further supports these findings by highlighting variations in the RC time constant, which reflect differences in charge storage efficiency between virgin and recycled plastics²⁵. Mid-infrared spectroscopy shows variations in spectral peaks that correlate with the percentage of recycled components in the plastics^{26,27}. Processing this multi-modal dataset using a machine learning framework and training an artificial intelligence (AI) model on the acquired triboelectric, dielectric, impedance, and spectroscopic data, we achieve over 90% accuracy in classifying PET samples with recycled content ranging from 0% to 100%. This result underscores the potential of our approach as a scalable, cost-effective solution for characterizing the percentage of recycled plastic in a plastic product.

Results

Different techniques that were used to generate orthogonal information for analysis by AI are described below.

Triboelectric current generation

The triboelectric effect, which involves contact electrification between surfaces, provides a useful method for studying the electrical behavior of polymeric materials²⁸. A custom-built triboelectric system in a parallel plate geometry, as shown in Fig. 2a, was used to analyze the triboelectric voltage behavior of plastics with varying amounts of recycled content. Here, the top electrode moves cyclically at a controllable speed against the stationary bottom electrode with the plastic sample. The measured triboelectric voltage characteristics for plastics with different recycled content are shown in Fig. 2b. To characterize the triboelectric voltage behavior, the response was modeled as exponential with a response time as shown in Fig. S1. PET samples with varying recycled plastic content were tested, and the response time constant was plotted as a function of recycled plastic percentage (Fig. 2c). The data shows that the time constant increases as a function of the percentage of recycled content, indicating slower charge dissipation.

Further experiments were conducted to examine the influence of electrode movement speed on triboelectric signal response. Virgin PET and PET containing 50% recycled content were tested at varying speeds to evaluate signal stability and amplitude, as shown in Fig. 2d. As the movement speed increased, the output signal intensity also increased; however, greater fluctuations were observed, indicating variability in the contact electrification dynamics. Based on these results, an optimal movement speed of 15 mm/s was selected for subsequent experiments to balance signal strength and stability. Triboelectric response of plastics provides the first multi-modal data component for determining the percentage of recycled content.

Dielectric/impedance analysis

Dielectric spectroscopy is a widely used technique for material characterization, particularly for assessing the electrical polarization, energy storage capability, and loss mechanisms in polymeric materials²⁹. The dielectric constant, a complex quantity, provides insight into the material's interaction with an applied electric field³⁰. It is expressed as $\epsilon = \epsilon' - j\epsilon''$, where ϵ represents the material's ability to store and remit energy in response to an alternating electric field, and ϵ'' describes the energy dissipation as heat within the material, which corresponds to dielectric loss. The ratio of the imaginary to real component defines the loss tangent δ , which quantifies the energy lost relative to the stored energy in the material³¹ $\tan \delta = \frac{\epsilon''}{\epsilon'}$. A higher loss tangent indicates increased energy dissipation under an applied field, making it a crucial parameter for evaluating the electrical behavior of recycled plastics. Higher dielectric loss is seen as undesirable for insulating materials, however, here it provides a measurable signature of recycled plastic defects³².

Recycled polymers contain inherent electrically active defects such as chain scissions, broken bonds, oxidation-induced impurities, and residual fillers from previous processing^{33,34}. These structural modifications introduce localized dipoles that differ from conventional free-electron hopping mechanisms observed in conductive materials^{35–37}. Unlike freely moving charge carriers, defect-induced dipoles are bound within the polymer matrix and respond to the external electric field by realigning or relaxing over time. This behavior results in a modified permittivity and dielectric loss, making dielectric spectroscopy a valuable tool for characterizing the degree of recycling in plastics.

To investigate the dielectric properties of recycled plastics, PET samples with varying proportions of recycled content were analyzed using an impedance analyzer (Keysight E4990A) operating in the 20 Hz–100 kHz range. The experimental setup consisted of two fixed capacitor plates mounted on an adjustable stage to maintain a consistent inter-electrode distance during testing. The impedance measurements were conducted using a linear frequency sweep mode from 1 kHz to 100 kHz with a precision setting of five. Before initiating the

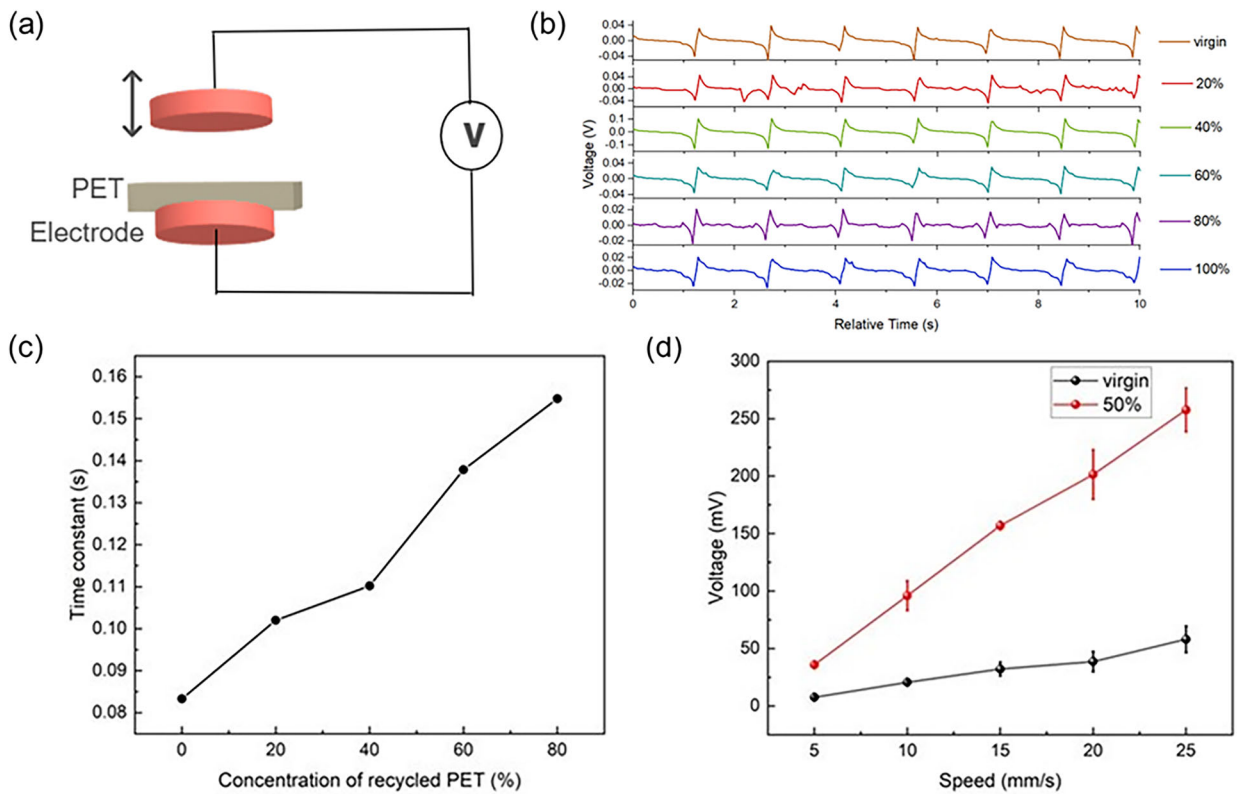


Fig. 2 | Triboelectric response of PET with varying recycled content. **a** Schematics of the custom-built triboelectric system. **b** Calculated discharge time constant of PET containing various percentages of recycled components. **c** Corresponding charging and discharging curves of PET containing various percentages of recycled

components. **d** The response of virgin PET (top) and PET containing 50% recycled content at varying speeds. Error bars represent the mean \pm standard deviation (s.d.) from five independent repeated measurements at each speed ($n = 5$).

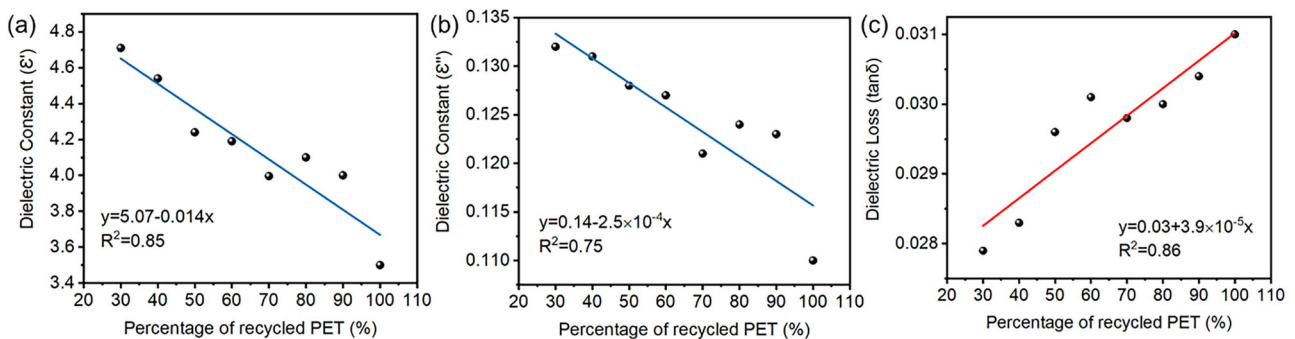


Fig. 3 | Dielectric/impedance analysis of PET with various percentages of recycled components. **a** Real part of the dielectric constant of PET with various recycled components at a fixed frequency of 30 kHz. **b** Imaginary part of the dielectric

constant of PET with various recycled components at a fixed frequency of 30 kHz. **c** Dielectric loss of PET with various recycled components at a fixed frequency of 30 kHz.

experiments, the impedance analyzer was calibrated using standard Open-Short compensation. The absolute impedance $|Z|$ and phase angle θ were recorded directly from the analyzer.

PET samples with different recycled content were analyzed, and the variations in their dielectric responses across the frequency spectrum were collected and presented in Fig. S2. Figure 3a–c shows the correlation between the recycled content and dielectric properties obtained at a fixed frequency of 30 kHz as a function of the percentage of recycled components. As shown in Fig. 3a, b, both the real (ϵ') and imaginary (ϵ'') parts of the dielectric constant decrease as the recycled plastic content increases. This trend suggests a reduction in the polarization ability of the material, which is indicative of diminished charge separation and lower energy storage efficiency in the presence of an electric field³⁸. The decrease in the real part (Fig. 3a) and the imaginary part (Fig. 3b) of the dielectric constant with

higher recycled content can be attributed to defects and impurities that disrupt long-range dipolar interactions, leading to lower permittivity. The reduction in charge separation suggests that the samples exhibit improved energy storage efficiency with minimal heat dissipation, which may have implications for applications requiring stable dielectric properties³⁷.

An increase in dielectric loss was observed with higher percentages of recycled plastic as shown in Fig. 3c, suggesting a significant phase difference between the applied electric field and the polarization response. This trend indicates that recycled plastics exhibit enhanced energy dissipation due to structural changes introduced during recycling. The increase in dielectric loss may be attributed to the presence of impurities, chain scissions, and oxidation-induced defects, which introduce additional relaxation processes within the polymer matrix. These defects disrupt the homogeneity of the dielectric response, leading to greater energy dissipation when the material is

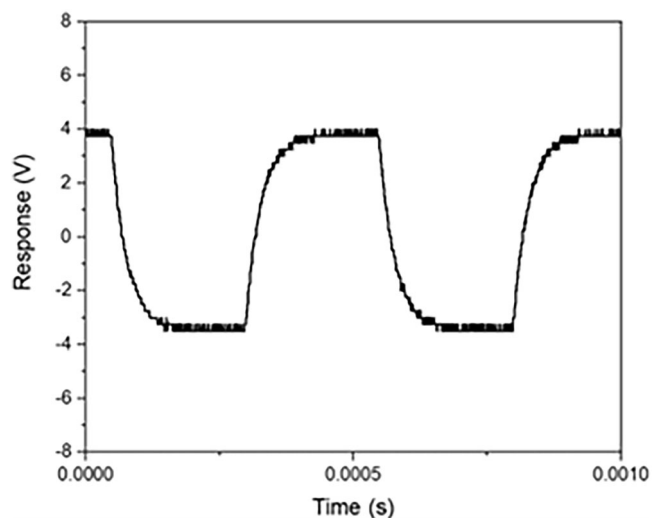


Fig. 4 | Charging-discharging response of the virgin PET sample in capacitance measurement. Voltage response of the PET virgin sample as a function of time during cyclic charging and discharging. The periodic voltage change reflects the capacitive behavior of the sample under alternating electrical excitation.

subjected to an alternating electric field. The observed reduction in permittivity and increase in dielectric loss with increasing recycled content are due to defect polarization and charge trapping in polymers. The dielectric response of plastics provides the second multi-modal data component for determining the percentage of recycled content.

Capacitance analysis for recycled plastic characterization

Capacitance analysis is an effective means of evaluating the dielectric properties of materials by examining the charging and discharging behavior of a capacitor. The charging and discharging rate of a capacitor in a series resistor-capacitor (RC) network is characterized by its RC time constant, τ , provides the dielectric response of the material within the capacitor. The RC time constant is defined as $\tau = R \cdot C$, where R is the resistance in the circuit and C is the capacitance. The capacitance of a system is directly influenced by the dielectric properties of the material placed between the capacitor plates. By applying a square wave voltage and monitoring the capacitor's response, the charging and discharging curves can be analyzed to extract τ , providing a quantitative metric for assessing the dielectric behavior of materials with varying recycled content. In a capacitor, the charging process occurs when an applied voltage causes charge accumulation on the plates, while the discharging process involves the release of stored charge³⁹. The rate at which these processes occur depends on the dielectric constant of the material, with materials of higher dielectric constant exhibiting longer charge retention times. Recycled plastics contain structural modifications such as polymer chain scission, oxidation-induced defects, and residual additives, all of which can influence the material's permittivity and, consequently, its capacitance. Since capacitance plays a fundamental role in determining the RC time constant, this analysis serves as a sensitive approach to detecting variations in plastic composition due to recycling.

To investigate the relationship between recycled content and dielectric properties, capacitors were constructed using plastic samples as the dielectric material. A function generator supplied a 1 kHz square wave voltage, and the capacitor's response was recorded using an oscilloscope. The experimental setup effectively functioned as a series RC circuit, enabling precise measurement of the RC time constant.

The experimental configuration ensured that the plastic samples were placed between two conductive plates, forming a parallel-plate capacitor where the permittivity of the plastic directly influenced the capacitance. The charging and discharging voltage profiles were recorded in real time, and the RC time constant was extracted by fitting the exponential decay of the discharge curve. $V(t) = V_0 e^{-t/\tau}$, where V_0 is the

initial voltage, $V(t)$ is the voltage at time t , and τ is the characteristic time constant governing the rate of voltage decay. This relationship allowed for a direct comparison between different plastic compositions based on their capacitance-induced charge retention behavior.

The charging and discharging curve for the PET virgin sample is shown in Fig. 4. PET samples with varying percentages of recycled content exhibited distinct variations in their RC time constants, as shown in the supplementary information. The calculated RC time constant for virgin PET was 13 μ s, with comparable variations observed across the tested samples. These differences underscore the sensitivity of capacitance analysis in detecting subtle changes in material composition. The variation suggests that recycled plastics, with their increased defect density, display weakened charge storage efficiency, leading to various discharge rates in the RC circuit. The results demonstrate that capacitance analysis provides a non-destructive and quantitative method for assessing the dielectric properties of recycled plastics. The observed variations in RC time constant offer valuable insight into the structural and electrical differences introduced by recycling. The capacitance analysis of plastics provides the third multi-modal data component for determining the percentage of recycled content.

Investigation of the spectroscopic signature of plastics with recycled components

Infrared spectroscopy is an excellent tool for the molecular and chemical composition of recycled plastics. Fourier transform infrared (FTIR) spectroscopy is used for the characterization of waste plastics⁴⁰, crystallinity of material⁴¹, and changes after recycling²⁰. The FTIR technique is well established to characterize polymers, and its ability to detect subtle degradation makes it useful for analyzing recycled plastics.

Attenuated total reflectance Fourier transform infrared (ATR-FTIR) spectroscopy was carried out on the PET films using a diamond prism with 5 scans and a resolution of 2 cm^{-1} . ATR-FTIR spectra of virgin PET and recycled PET are shown in Fig. 5a–d. No difference was seen between the spectra of both sides of virgin PET and recycled PET. They represent a general PET structure. However, as shown in Fig. 5a–c, absorption bands in virgin PET at 844, 973, 1470 cm^{-1} , are significantly weaker in recycled PET, corresponding to trans CH_2 rocking, $\text{O}-\text{CH}_2$ or $\text{C}(=\text{O})-\text{O}$ and CH_2 bending⁴². More specifically, they are associated with a structure derived from ethylene glycol.

It is known that the recycling process can induce degradation, including chain scission⁴³. However, the change in the above absorption bands indicates the elimination or modification of ethylene glycol. It is suggested that the number of ethylene glycol groups as a terminal of the polymer chain has changed⁴⁴. López et al. indicated that chain scission during PET recycling often generates polymer radicals with hydroxyl groups. However, as shown in Fig. 5d, the given recycled PET shows a lower intensity of the absorption band at 3430 cm^{-1} , corresponding to the hydroxyl groups, than virgin PET, suggesting that the recycling process does not necessarily generate hydroxyl groups.

Furthermore, all these changes can be associated with changes in crystallinity⁴⁵. In other words, the FTIR result also indicates that the degree of crystallinity of PET may be lowered after the recycling process. When the crystallinity is lowered, the ductility and processability of the polymer can be degraded⁴⁶. The spectroscopic signature of plastics provides the fourth multi-modal data component for determining the percentage of recycled content.

Multi-modal deep learning classification using all modalities. The physical methods discussed in the previous section provide insight into the physical characteristics of the plastic object being tested. However, the composite information is high-dimensional, and the differences in the signals are nuanced. Further, due to experimental challenges like the (i) availability of high-quality recycled PET samples with the known recycled percentages and (ii) multi-modal measurement for each sample, the number of samples is limited, which makes the application of modern machine learning challenging for this task.

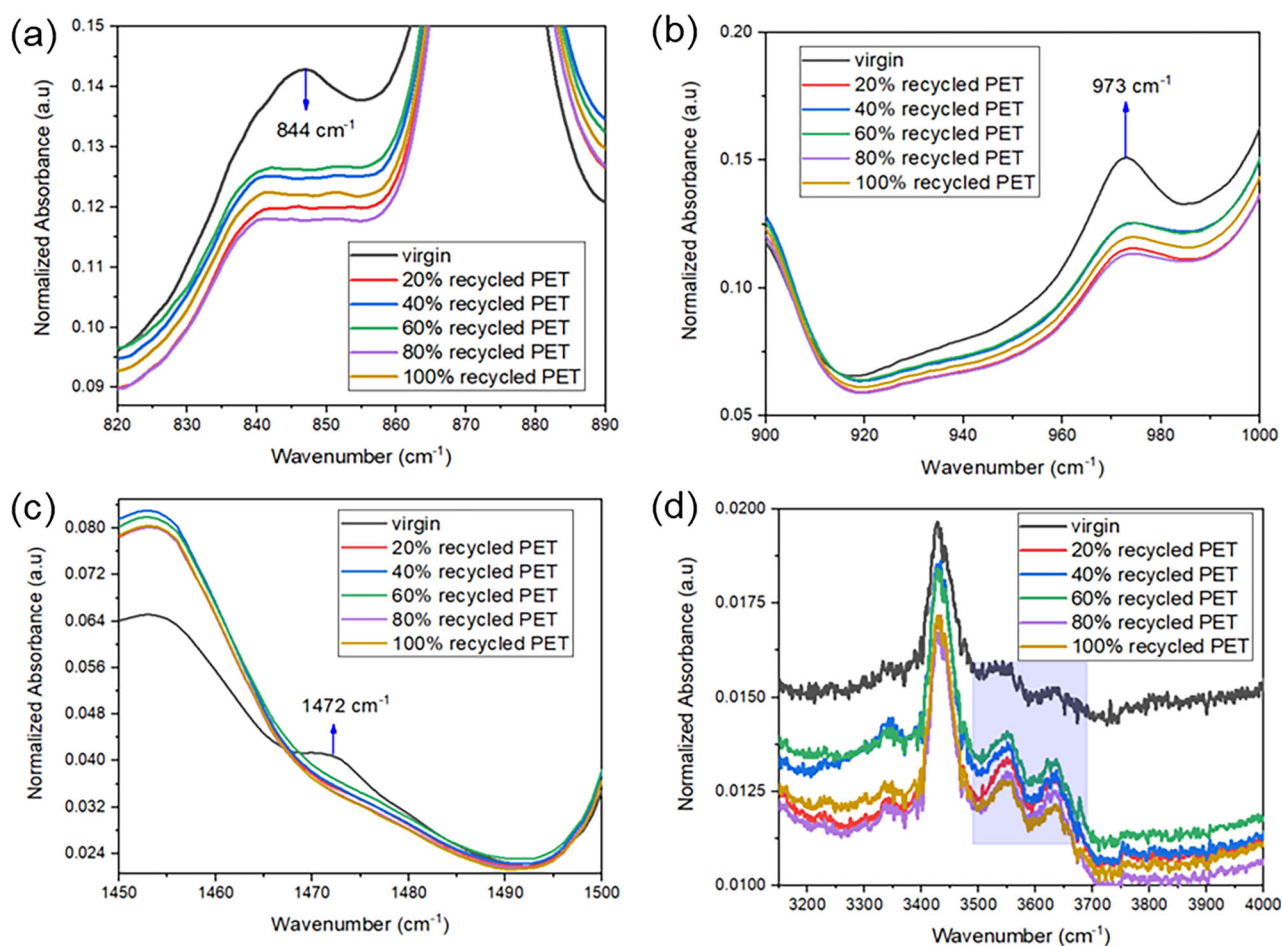


Fig. 5 | ATR-FTIR spectra of virgin PET and recycled PET samples in different wavenumber ranges. **a** 820–890 cm^{-1} , **b** 900–1000 cm^{-1} , **c** 1450–1500 cm^{-1} , and **d** 3200–4000 cm^{-1} .

To address the challenges pertaining to high-dimensional information, we preprocess and encode each modality based on our understanding of the sensing mechanism and combine all four sensing modalities using modern machine learning (deep discriminator network) for the most accurate identification of the percentage of plastic in each sample. To address the challenge in data availability, we perform modality-specific data augmentation to allow us to employ data-driven approaches to classification.

In this section, we discuss the design, training, and evaluation of our deep discriminator network, trained as a single classification model over all eleven classes using all four modalities, as well as the data augmentation, pre-processing, and encoding required to successfully train our classifier. Finally, we discuss the contribution of each of the individual modalities in differentiating the various types of recycled plastic samples. The details of the learning-based analysis are discussed in the Supplementary Materials section.

Figure 6 and Table 1 detail the architecture of our deep classifier network with a convolutional neural network (CNN) encoding head for the FTIR modality. CNNs have been used in the past to classify different kinds of plastics^{46,47}. We use 1D convolutional layers to encode the high-dimensional FTIR modality into a smaller embedding space. We then concatenate the encoded features of the other modalities (peaks from triboelectric charging and discharging response, dielectric constants from impedance analysis, and SEM features from capacitance response), indicated as VIC in Fig. 6, to the embeddings. These augmented features are then further reduced using a fully connected classification head. The 1D convolutional layers encode the high-dimensional FTIR modality into a vector

encoding. For each of the other modalities, voltage, impedance, and capacitance, the feature extraction pre-processing step serves as the encoder.

FTIR spectra of materials have previously been modeled as a baseline spectrum, characterizing each material type, shifted by linear combinations of noise factors to account for aleatoric and epistemic uncertainties⁴⁸. For example, the EMSC method⁴⁹ models the spectra as:

$$A(\hat{\nu}) = a + m(\hat{\nu}) + b + d_1\hat{\nu} + d_2\hat{\nu}^2 + \dots + d_n\hat{\nu}^n$$

Where $A(\hat{\nu})$ is the measured spectrum, $m(\hat{\nu})$ is the reference spectrum, and $a, b, d_1, d_2, \dots, d_n$ are the parameters for the baseline shift and multiplicative effect of higher order polynomials. In this work, we use a first order polynomial approximation for the data augmentation. For other modalities, we augment the extracted features like voltage peak heights and widths, impedance dielectric constants, etc. by fitting Gaussian distributions using sample statistics. Details of this feature extraction are discussed in the next section.

Our proposed model has an accuracy of 92% over the testing set with an F_1 score of 0.95. We utilize a test set ratio of 0.3 over our augmented dataset of 22000 samples for all our experiments. We show the confusion matrix of the predictions in Fig. 6. We see that 0–50% and 100% plastics are almost perfectly classified. The network has confusion between 70 and 90% plastics. We note from previous sections that the FTIR is the most impactful modality, followed by the dielectric constants from the impedance analysis and the triboelectric charging and discharging responses. We study classification with each modality in isolation in the next section.

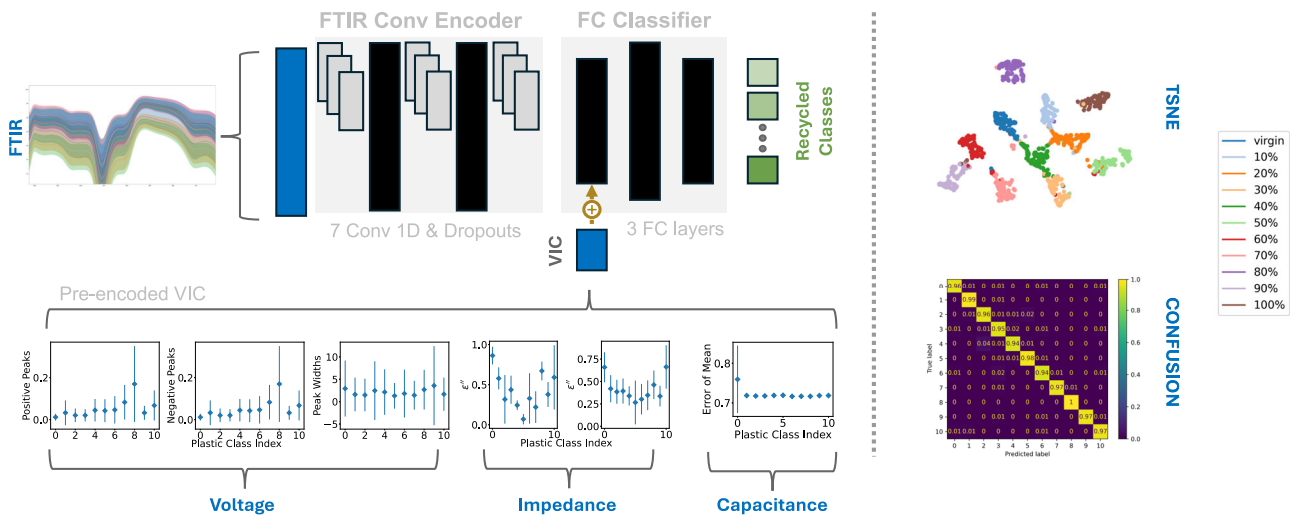


Fig. 6 | Proposed Deep Learning architecture. The model uses 1D convolutional layers to transform FTIR into a latent embedding and combines with voltage, impedance, and capacitance modalities for classification. tSNE embedding and

confusion matrix show effective classification performance. Plots for voltage, impedance, and capacitance indicate mean and standard deviation in measurements over samples.

Table 1 | Proposed deep learning architectural details

Layer	Size	Dropout	Pooling
Conv 1D	1 × 8 × 3	Dropout 0.1	
Conv 1D	8 × 8 × 1	Dropout 0.05	
Conv 1D	8 × 8 × 3	Dropout 0.1	MaxPool 1D (3)
Conv 1D	8 × 8 × 1	Dropout 0.05	
Conv 1D	8 × 8 × 3	Dropout 0.1	
Conv 1D	8 × 8 × 3	Dropout 0.1	MaxPool 1D (3)
Conv 1D	8 × 8 × 3	Dropout 0.1	MaxPool 1D (3)
Flatten			
FC	37 × 24	Dropout 0.1	
FC	24 × 16	Dropout 0.1	
FC	16 × 11		

FTIR modalities is encoded with a series of 1D Convolutional layers. Extracted features for Voltage, Impedance and Capacitance modes are concatenated to the FTIR encoding before the classification head. Dropouts are used for regularization.

The ability to rapidly screen plastic products for recycled content has significant implications for regulatory compliance, material quality assurance, and sustainable manufacturing. Future research will focus on refining the methodology, expanding the applicability to different polymer types, and integrating real-time sensing capabilities into a portable diagnostic device for field applications. By developing an accessible and highly accurate technique for quantifying recycled content, this work contributes to the advancement of a circular economy by facilitating the reuse of recycled plastics and reducing environmental waste.

Classification with each sensing modality in isolation—A study

In the previous section, we demonstrated our proposed classification model that discriminates all eleven classes using a combination of all four modalities. In this section, we study classification with each modality in isolation by separately training individual classifiers for each modality^{50–52} and analyzing their performance on the various recycled plastics classes.

Modal 1—Investigating the impact of spectroscopic signature in classification

The FTIR modality is the most feature-rich and most impactful modality in terms of classification. Correspondingly, it is also the most popular in contemporary literature for deep learning-based classification of various

materials like plastics, proteins, pharmaceuticals, etc. From qualitative observation, the signals are different in windows of wavenumbers for differing percentages of plastics. Wavenumber ranges of 800–900, 900–1000, and 1450–1500 are of particular interest. For our classification, we use the ranges 800–1000. For data augmentation, for each recycled plastic type (10%, 20%, etc.), we use the mean of the measured samples for the respective plastic type as the reference spectra and add a small amount of random positive or negative additive shift to the spectra within the range of its variation for the respective plastic type. Finally, we add a small white noise to the individual wave numbers for the purpose of regularization in deep learning. Using this data augmentation, we increase the number of samples from 220 to 22,000 samples. Unlike other modalities in the previous sections, we use a 1D Convolutional Neural Network instead of a Gaussian Process Classifier to handle the higher dimensionality in the classification process. Using only the FTIR data in this range, we obtain a classification accuracy of 65%. We attribute this performance to the successful classification of 10%, 30–70%, 90%, and 100% plastics, as shown in Fig. 7, which depicts the t-distributed stochastic neighborhood embedding (tSNE) that shows the separation of plastics of various percentages of recycled components after classification in the embedding space. In this visualization, tighter clustering of the same type of sample and better separation of these clusters indicates better classification.

Modal 2—Classification with dielectric/impedance in isolation

Performing a qualitative observation of the real and imaginary parts of the dielectric constants ϵ' and ϵ'' , we see that there are clear variations of the dielectric constants for these plastic types, as shown in Fig. 6. We extract the real and imaginary parts of the dielectric constants for the deep learning discriminator network. We use sample statistics (mean and standard deviation in ϵ' and ϵ'') to generate augmented samples to increase the data from 110 to 22,000 samples and enhance the training of our network. Using a Gaussian Process Classifier⁴⁵ on these features, we find that plastics with 10%, 40%, 50% recycled components are the most differentiated while 80–100% classes are reasonably discriminated using this modality, as observed in the tSNE plot in Fig. 7.

Modal 3—classification with triboelectric charging and discharging in isolation

From qualitative observation of the non-normalized triboelectric charging and discharging curves, the peak heights and peak widths of the voltage for plastics with different percentages of recycled components are different, especially so for the 80% recycled plastic class. We extract the positive and

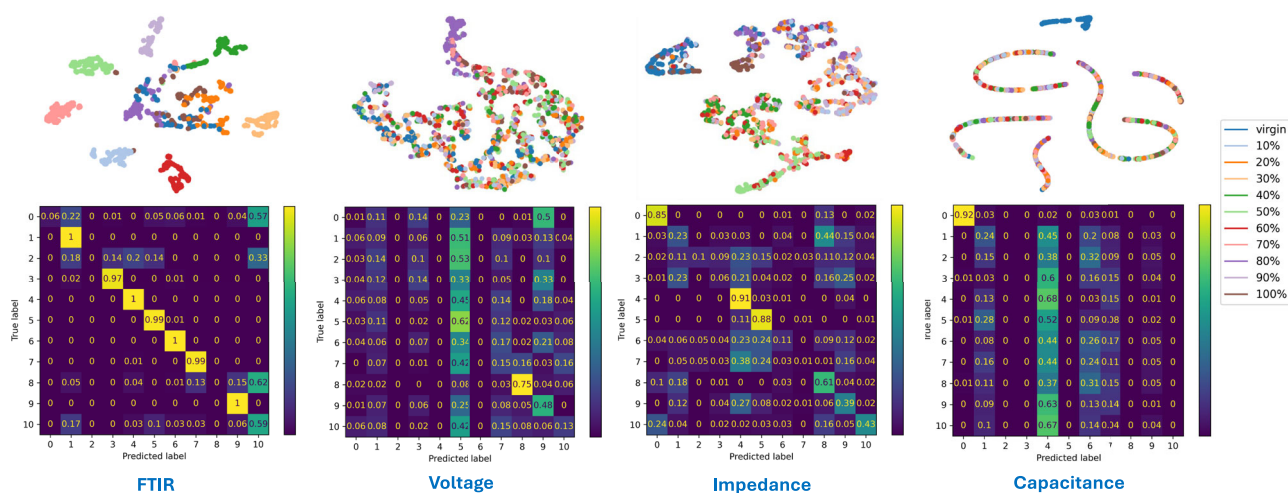


Fig. 7 | tSNE and confusion matrix of Gaussian Process classifiers trained on individual modalities to study their utility in isolation. Results indicate that FTIR and Impedance are the most impactful modalities followed by voltage and capacitance.

negative peak heights and peak widths for the deep learning discriminator network. This serves as the encoding method for the voltage modality. We then use sample statistics (mean and standard deviation of peak heights and widths) to generate augmented samples to significantly increase the number of samples from 110 to 22,000 and make the data amenable to learning-based classification. Note, from Fig. 7, that plastics with 80% recycled components are the most differentiated using this modality.

Modal 4—classification with capacitance analysis in isolation

In observing the capacitance, the variation in the signal responses for different types of samples is within the noise range of the individual sample types. Therefore, we incorporate the cumulative standard error of the mean (SEM) statistic into our discriminator network to capture subtle and nuanced changes in these values. We use these sample statistics to generate augmented samples to increase the data from 110 to 22,000 and enhance the training of our network. The tSNE distribution in Fig. 7 for this modality after classification indicates that capacitance is useful to discriminate virgin plastics.

The techniques used in this study offer a range of spatial resolutions and depth sensitivities. While impedance and capacitance techniques provide bulk-averaged information across the sample thickness, ATR-FTIR is a surface-sensitive technique with a micrometer-scale penetration depth. The triboelectric measurements represent a mesoscale surface interaction. In real-world applications with potentially non-uniform recyclate distribution, measurements across multiple regions and depths may be required for representative assessment. Additionally, poor compounding may manifest as broadened or multimodal signals in dielectric and triboelectric responses.

The current model was developed using mechanically recycled PET from a single, bottle-grade source. While this provides controlled data for model training, broader deployment will require expansion to PET from textiles, thermoforms, and other post-consumer sources. Future work will incorporate samples from diverse recycling streams and explore transfer learning strategies to improve generalizability across polymer types and feedstock heterogeneity.

Conclusions

In this work, we present a multi-modal, non-destructive sensing technique to quantify the percentage of recycled plastic content in plastic products, addressing a critical gap in sustainable plastic recycling. By integrating triboelectric analysis, dielectric and impedance spectroscopy, capacitance measurements, and mid-infrared spectroscopy with machine learning, we achieved over 97% classification accuracy across PET samples ranging from 0% to 50% recycled content, which is the expected regime of required recycled content in plastic products. The integration of these orthogonal

signals through deep learning enables accurate prediction of recycled content in a scalable and cost-effective manner. This approach holds strong potential for regulatory compliance, quality assurance, and advancing circular economy initiatives by enabling real-time, in situ evaluation of recycled plastic content in consumer and industrial products.

Experimental methods

Sample preparation

The PET samples used in this study were supplied by Plastic Technologies Inc. (PTI) and were fabricated under controlled conditions to ensure uniformity and reproducibility. The source of the recycled PET (rPET) was post-consumer bottles, and all recycled content was produced through mechanical recycling processes. These steps typically include de-baling, material sortation, optional pre-washing, grinding, hot washing, elutriation, and extrusion into pellets.

A commercially available rPET resin that is used commonly in the beverage industry was used to fabricate the samples at PTI. The particular rPET resin chosen by PTI was supplied by a US based reclaimer whose product is considered average with respect to rPET resins currently available. It is neither more clean nor more dirty than the average rPET being used to produce beverage preforms and bottles. The exact processes used to produce the rPET are proprietary to that reclaimer but are consistent with the industry standards and generate a food grade rPET resin covered by a letter of non-objection from the FDA.

To prepare the final experimental materials, recycled and virgin PET resins were blended at PTI using a bag shaker/bag tumbler, a standard method that ensures uniform mixing of pelletized materials before extrusion and film fabrication. This approach produced PET films with known recycled content ranging from 0% to 100%, with homogeneous distribution of the recycled fraction confirmed through the controlled manufacturing process.

The recycled PET samples were assumed to be free from significant impurities or fillers, as they had undergone comprehensive mechanical cleaning and sortation.

This study focused exclusively on mechanically recycled PET, which retains the polymer backbone but accumulates structural and morphological defects, such as chain scission and oxidation, that are detectable through our multi-modal sensing framework. Although this work did not include chemically recycled PET, we note that chemically recycled materials can also exhibit minor deviations from virgin PET due to repolymerization variability or processing history. The sensing and classification method developed here is adaptable and can be extended to other forms of recycled PET, including chemically recycled PET, by retraining the model with appropriately labeled datasets. This flexibility supports the potential use of

our technique in distinguishing virgin, mechanically recycled, and chemically recycled materials, and in identifying subtle quality differences across a range of plastic products.

Data availability

The authors declare that access to the “minimum dataset” that are necessary to interpret, verify and extend the research in the article within the paper and its Supplemental Information files will be made available upon request to the authors. The data to train and test the Deep Learning classifier can be downloaded from <https://drive.google.com/file/d/1dQpPcZvKatIxHsIM1J-Ny083GwXibxJ9/view?usp=sharing>.

Code availability

The code to train and test the Deep Learning classifier can be downloaded from <https://drive.google.com/file/d/1dQpPcZvKatIxHsIM1J-Ny083GwXibxJ9/view?usp=sharing>. Upon acceptance, the authors will share the code and data through a permanent institutional link.

Received: 30 May 2025; Accepted: 26 February 2026;

Published online: 23 March 2026

References

- Thomas, D. S., Kneifel, J. D. & Butry, D. T. The US Plastics Recycling Economy. (2024).
- Committee, I. N. *First part of the Fifth Session (INC-5.1)*, <https://www.unep.org/inc-plastic-pollution/session-5> (2024).
- Committee, I. N. *Second part of the Fifth Session (INC-5.2)*, <https://www.unep.org/inc-plastic-pollution/session-5.2> (2025).
- Saviello, D., Toniolo, L., Goidanich, S. & Casadio, F. Non-invasive identification of plastic materials in museum collections with portable FTIR reflectance spectroscopy: Reference database and practical applications. *Microchem. J.* **124**, 868–877 (2016).
- Mansa, R. & Zou, S. Thermogravimetric analysis of microplastics: A mini review. *Environ. Adv.* **5**, 100117 (2021).
- Lynch, J. M. et al. Differential scanning calorimetry (DSC): An important tool for polymer identification and characterization of plastic marine debris. *Environ. Pollut.* **346**, 123607 (2024).
- Zhou, Z. et al. Recent advances and applications of nmr techniques in plastic characterizations. *Anal. Chem.* **97**, 5847–5865 (2025).
- Milisavljević, J. et al. in *Danubia-Adria Symposium, University Of Belgrade, Serbia*. 266–269.
- Hirose, Y., Hata, K., Sugawara, M. & Takei, M. Sensing performance of dielectric sensor in mixed melting polymer pellets for waste plastic separation. *Adv. Powder Technol.* **26**, 1687–1695 (2015).
- Perkins, W. G. Polymer toughness and impact resistance. *Polym. Eng. Sci.* **39**, 2445–2460 (1999).
- Carvel, R., Steinhaus, T., Rein, G. & Torero, J. Determination of the flammability properties of polymeric materials: A novel method. *Polym. Degrad. Stab.* **96**, 314–319 (2011).
- Schyns, Z. O. G., Bennett, T. M. & Shaver, M. P. Recycled Plastic Content Quantified through Aggregation-Induced Emission. *ACS Sustain. Chem. Eng.* **10**, 12659–12669 (2022).
- Richards, B. Inorganic fluorescent marker materials for identification of post-consumer plastic packaging. *Resources, Conservation and Recycling* **161** <https://doi.org/10.1016/j.resconrec.2020.104976> (2020).
- Diaz Sotil, A. E. Analysis of standards and certification protocols for verifying recycled content in plastic products. <https://doi.org/10.11575/PRISM/40200> (2022).
- Esmaeilzade, R. et al. Correlation of structure, rheological, thermal, mechanical, and optical properties in low density polyethylene/linear low density polyethylene blends in the presence of recycled low density polyethylene and linear low density polyethylene. *Polym. Eng. Sci.* **64**, 1286–1298 (2024).
- Lamtai, A., Elkoun, S., Robert, M., Mighri, F. & Diez, C. Mechanical recycling of thermoplastics: A review of key issues. *Waste* **1**, 860–883 (2023).
- Mendes, A. A., Cunha, A. M. & Bernardo, C. A. Study of the degradation mechanisms of polyethylene during reprocessing. *Polym. Degrad. Stab.* **96**, 1125–1133 (2011).
- Reck, B. K. & Graedel, T. E. Challenges in metal recycling. *Science* **337**, 690–695 (2012).
- Grigorescu, R. M., Grigore, M. E., Iancu, L., Ghioca, P. & Ion, R.-M. Waste electrical and electronic equipment: A review on the identification methods for polymeric materials. *Recycling* **4**, 32 (2019).
- Signoret, C., Caro-Bretelle, A.-S., Lopez-Cuesta, J.-M., Lenny, P. & Perrin, D. Alterations of plastics spectra in MIR and the potential impacts on identification towards recycling. *Resour., Conserv. Recycl.* **161**, 104980 (2020).
- Neo, E. R. K., Yeo, Z., Low, J. S. C., Goodship, V. & Debattista, K. A review on chemometric techniques with infrared, Raman and laser-induced breakdown spectroscopy for sorting plastic waste in the recycling industry. *Resour. Conserv. Recycl.* **180**, 106217 (2022).
- Feng, X., Li, Q. & Wang, K. Waste plastic triboelectric nanogenerators using recycled plastic bags for power generation. *ACS Appl. Mater. Interfaces* **13**, 400–410 (2021).
- Wang, S. et al. Polymer-based dielectrics with high permittivity and low dielectric loss for flexible electronics. *J. Mater. Chem. C.* **10**, 6196–6221 (2022).
- Qiu, J. et al. Preparation and application of dielectric polymers with high permittivity and low energy loss: A mini review. *J. Appl. Polym. Sci.* **139**, 52367 (2022).
- Xia, S. & Chen, L. Theoretical and experimental investigation of optimal capacitor charging process in RC circuit. *Eur. Phys. J.* **132**, 235 (2017).
- Zhao, Y. et al. Molecular characterization of plastic waste using standoff photothermal spectroscopy. *ECS Sens.* **2**, 043401 (2023).
- Signoret, C. et al. MIR spectral characterization of plastic to enable discrimination in an industrial recycling context: III. Anticipating impacts of ageing on identification. *Waste Manag.* **109**, 51–64 (2020).
- Wang, Z. L. From contact electrification to triboelectric nanogenerators. *Rep. Prog. Phys.* **84**, 096502 (2021).
- Wei, J. & Zhu, L. Intrinsic polymer dielectrics for high energy density and low loss electric energy storage. *Prog. Polym. Sci.* **106**, 101254 (2020).
- Zhu, L. Exploring strategies for high dielectric constant and low loss polymer dielectrics. *J. Phys. Chem. Lett.* **5**, 3677–3687 (2014).
- White, A. J. Loss analysis of thermal reservoirs for electrical energy storage schemes. *Appl. Energy* **88**, 4150–4159 (2011).
- Chao, H. W., Chen, H. H. & Chang, T. H. Measuring the complex permittivities of plastics in irregular shapes. *Polymers (Basel)* **13**. <https://doi.org/10.3390/polym13162658> (2021).
- Tian, R., Li, K., Lin, Y., Lu, C. & Duan, X. Characterization techniques of polymer aging: from beginning to end. *Chem. Rev.* **123**, 3007–3088 (2023).
- Mihelčić, M., Oseli, A., Huskić, M. & Slemenik Perše, L. Influence of stabilization additive on rheological, thermal and mechanical properties of recycled polypropylene. *Polymers (Basel)* **14**. <https://doi.org/10.3390/polym14245438> (2022).
- DeArmitt, C. & Hancock, M. 357–424 (2003).
- Kremer, F. & Schönhal, A. *Broadband dielectric spectroscopy*. (Springer Science & Business Media, 2002).
- Ieda, M. Dielectric breakdown process of polymers. *IEEE Transactions on Electrical Insulation*, 206–224 (1980).
- Gao, L., He, J., Hu, J. & Li, Y. Large enhancement in polarization response and energy storage properties of poly(vinylidene fluoride) by improving the interface effect in nanocomposites. *J. Phys. Chem. C.* **118**, 831–838 (2014).

39. Guan, L., Yu, L. & Chen, G. Z. Capacitive and non-capacitive faradaic charge storage. *Electrochim. Acta.* **206**, 464–478 (2016).
40. Fan, C., Huang, Y.-Z., Lin, J.-N. & Li, J. Microplastic constituent identification from admixtures by Fourier-transform infrared (FTIR) spectroscopy: The use of polyethylene terephthalate (PET), polyethylene (PE), polypropylene (PP), polyvinyl chloride (PVC) and nylon (NY) as the model constituents. *Environ. Technol. Innov.* **23**, 101798 (2021).
41. Tretinnikov, O. & Zagorskaya, S. Determination of the degree of crystallinity of poly (vinyl alcohol) by FTIR spectroscopy. *J. Appl. Spectrosc.* **79**, 521–526 (2012).
42. López, M.dM. C. et al. Assessing changes on poly(ethylene terephthalate) properties after recycling: Mechanical recycling in laboratory versus postconsumer recycled material. *Mater. Chem. Phys.* **147**, 884–894 (2014).
43. Assadi, R., Colin, X. & Verdu, J. Irreversible structural changes during PET recycling by extrusion. *Polymer.* **45**, 4403–4412 (2004).
44. Sammon, C., Yarwood, J. & Everall, N. An FT–IR study of the effect of hydrolytic degradation on the structure of thin PET films. *Polym. Degrad. Stab.* **67**, 149–158 (2000).
45. Prasad, S. G., De, A. & De, U. Structural and optical investigations of radiation damage in transparent PET polymer films. *Int. J. Spectrosc.* **2011**, 810936 (2011).
46. Awaja, F. & Pavel, D. Recycling of PET. *Eur. Polym. J.* **41**, 1453–1477 (2005).
47. Hinton, G. E. & Roweis, S. Stochastic neighbor embedding. *Advances in neural information processing systems* **15** (2002).
48. Jiang, S. et al. Using ATR-FTIR spectra and convolutional neural networks for characterizing mixed plastic waste. *Comput. Chem. Eng.* **155**, 107547 (2021).
49. Zeng, G. et al. Deep convolutional neural networks for aged microplastics identification by Fourier transform infrared spectra classification. *Sci. Total Environ.* **913**, 169623 (2024).
50. Yan, X. et al. FRDA: Fingerprint region based data augmentation using explainable AI for FTIR based microplastics classification. *Sci. Total Environ.* **896**, 165340 (2023).
51. Kohler, A., Kirschner, C., Oust, A. & Martens, H. Extended multiplicative signal correction as a tool for separation and characterization of physical and chemical information in Fourier transform infrared microscopy images of cryo-sections of beef loin. *Appl. Spectrosc.* **59**, 707–716 (2005).
52. Williams, C. K. & Rasmussen, C. E. *Gaussian processes for machine learning*. Vol. 2 (MIT press Cambridge, MA, 2006).

Acknowledgements

The authors thank the New York State (NYS) Center for Plastics Recycling Research and Innovation at the University at Buffalo (UB) and the New York State Department of Environmental Conservation (NYSDEC) for support. The work was supported by a grant from New York State's Environmental Protection Fund administered by NYSDEC under a Memorandum of Understanding (MOU) AMI 12490 between NYSDEC and UB, Project and Center Director, Amit Goyal. Charuvahan Adhivarahan and Karthik Dantu were also partially supported by a gift from MOOG Inc. The authors thank Dan Durham and Shachi Vaish at PTI (<https://www.plastictechnologies.com>) for fabricating the custom samples with varying percentages of recycled content. The authors acknowledge useful discussions in biweekly meetings of the NYS Center for Plastics Recycling Research and Innovation team at

the University at Buffalo. The authors also acknowledge John Vana, Kathleen A. Prather, Gary Feinland, and the larger team at the NYSDEC for useful discussions. The opinions, findings, and/or interpretations of data contained therein are the responsibility of the University and do not necessarily represent the opinions, interpretations, or policy of the New York State Department of Environmental Conservation.

Author contributions

Y.Z. conducted the experimental work and took the lead in writing the paper. C.A. conducted the AI/ML work reported in the paper and co-wrote the paper. Y.Z. and C.A. contributed equally to the work. C.L.J. conducted the experiments. K.D. supervised the AI/ML work. T.T. developed the initial idea and lead the experimental work. A.G. obtained the funding, established the project and coordinated all aspects of the project. All authors reviewed the paper and made useful modifications. All other authors declare no competing interests including financial and non-financial interests.

Competing interests

The authors declare no competing interests.

Additional information

Supplementary information The online version contains supplementary material available at <https://doi.org/10.1038/s44172-026-00639-y>.

Correspondence and requests for materials should be addressed to Amit Goyal.

Peer review information *Communications Engineering* thanks Seshasayee Mahadevan and the other, anonymous, reviewer(s) for their contribution to the peer review of this work. Primary Handling Editors: [Wan-Ting (Grace) Chen] and [Rosamund Daw].

Reprints and permissions information is available at <http://www.nature.com/reprints>

Publisher's note Springer Nature remains neutral with regard to jurisdictional claims in published maps and institutional affiliations.

Open Access This article is licensed under a Creative Commons Attribution-NonCommercial-NoDerivatives 4.0 International License, which permits any non-commercial use, sharing, distribution and reproduction in any medium or format, as long as you give appropriate credit to the original author(s) and the source, provide a link to the Creative Commons licence, and indicate if you modified the licensed material. You do not have permission under this licence to share adapted material derived from this article or parts of it. The images or other third party material in this article are included in the article's Creative Commons licence, unless indicated otherwise in a credit line to the material. If material is not included in the article's Creative Commons licence and your intended use is not permitted by statutory regulation or exceeds the permitted use, you will need to obtain permission directly from the copyright holder. To view a copy of this licence, visit <http://creativecommons.org/licenses/by-nc-nd/4.0/>.

© The Author(s) 2026